Lithium Batteries Hot Paper

How to cite: *Angew. Chem. Int. Ed.* **2021**, *60*, 22791 – 22796
International Edition: doi.org/10.1002/anie.202106237
German Edition: doi.org/10.1002/ange.202106237

# Ionic Liquid Functionalized Gel Polymer Electrolytes for Stable Lithium Metal Batteries

*Tianhong Zhou[+], Yan Zhao[+], Jang Wook Choi,* and Ali Coskun**

***Abstract:*** *Metallic lithium (Li) is regarded as the ideal anode material in lithium-ion batteries due to its low electrochemical potential, highest theoretical energy density and low density. There are, however, still significant challenges to be addressed such as Li-dendrite growth and low interfacial stability, which impede the practical application of Li metal anodes. In order to circumvent these shortcomings, herein, we present a gel polymer electrolyte containing imidazolium ionic liquid end groups with a perfluorinated alkyl chain (F-IL) to achieve both high ionic conductivity and Li ion transference number by fundamentally altering the solubility of salt within the gel electrolyte through Lewis-acidic segments in the polymer backbone. Moreover, the presence of F-IL moieties decreased the binding affinity of Li cation towards the glycol chains, enabling a rapid transfer of Li cation within the gel network. These structural features enabled the immobilization of anions on the ionic liquid segments to alleviate the space-charge effect while promoting stronger anion coordination and weaker cation coordination in the Lewis-acidic polymers. Accordingly, we realized a high Li ion conductivity ($9.16\times10^{-3}$ S cm$^{-1}$) and high Li ion transference number of 0.69 simultaneously, along with a good electrochemical stability up to 4.55 V, while effectively suppressing Li dendrite growth. Moreover, the gel polymer electrolyte exhibited stable cycling performance of the Li | Li symmetric cell of 9 mAh cm$^{-2}$ for more than 1800 hours and retained 86.7 % of the original capacity after 250 cycles for lithium-sulfur (Li-S) full cell.*

## Introduction

The consumer demand for portable electronic devices, drones and all-electric vehicles has increased massively in recent years, and Li-ion batteries (LIBs) have played a pivotal role in this direction. Conventional LIBs are close to their theoretical limits in terms of attainable energy density, thus requiring new chemistries that allow to store Li ions far beyond today's LIBs that operate based on the intercalation mechanism. Metallic Li has been extensively studied as an anode material since the 1970s due to its high theoretical capacity (3860 mAh g$^{-1}$) and low electrode potential (−3.040 V versus standard hydrogen electrode).[1] Therefore, Li metal batteries (LMBs) that adopt Li metal anodes can be a game changer to overcome the energy density limitations of LIBs. There are, however, several inherent technological barriers to overcome, such as Li dendrite growth and resulting uncontrolled solid electrolyte interphase (SEI) formation. This interfacial instability is also associated with the high reactivity of metallic Li during cycling and overheating, which can potentially lead to a poor cycling performance and safety hazards.[2]

In an attempt to address these shortcomings, a variety of approaches have been employed; optimizing electrolyte additives,[3] introducing artificial SEI layers,[4] designing three-dimensional Li hosts[5] and implementing solid-state[6] and cross-linked gel polymer electrolytes (CGPEs),[7] etc. While the majority of these approaches have had a marked impact, the development of CGPEs incorporating glycol chains is remarkable owing to their potential to facilitate an effective, relatively homogeneous $Li^+$ flux while aiding to mitigate the Li dendrite growth and enabling control over the surface microstructure of Li metal.[8] Conventional CGPEs, which are dual ion conductors, generally show Li ion transference numbers ($t_{Li}^+$) below 0.5, an indication that the ionic conductivity is mainly governed by the free anion motion, leading to a concentration gradient of anions and further causing an exacerbated dendrite propagation when applied to a Li metal anode. With the same logic involved, in order to increase $t_{Li}^+$, the free movement of anions needs to be limited. Whereas single-ion conducting CGPEs incorporating anionic sites/traps exhibited $t_{Li}^+$ close to unity, they generally exhibited relatively low ionic conductivities. Therefore, the simultaneous realization of high ionic conductivity and $t_{Li}^+$ is the major bottleneck for the further evolution of CGPEs. The ionic conductivity of CGPEs is fairly critical for the operation of a battery cell at high rates as well as uniform Li (de)plating (from) onto the Li metal anodes for LMBs.[9] In this direction,

[*] T. Zhou,[+] Y. Zhao,[+] Prof. A. Coskun
Department of Chemistry, University of Fribourg
Chemin de Musee 9, 1700 Fribourg (Switzerland)
E-mail: ali.coskun@unifr.ch
Prof. J. W. Choi
School of Chemical and Biological Engineering, Department of Materials Science and Engineering, and Institute of Chemical Processes, Seoul National University
1 Gwanak-ro, Gwanak-gu, Seoul 08826 (Republic of Korea)
E-mail: jangwookchoi@snu.ac.kr
[+] These authors contributed equally to this work.
Supporting information and the ORCID identification number(s) for the author(s) of this article can be found under https://doi.org/10.1002/anie.202106237.

several promising approaches have been proposed—namely, adding plasticizers,[10] designing single-ion conducting CGPEs[11] and introducing self-healing ability.[12]

Ionic liquids (ILs) are salts that exist as liquids at low temperatures. They are also synthetically highly versatile and have also been studied to form a smooth Li plating morphology on the Li metal anode.[13] Aside from being the most electronegative element,[14] fluorine atoms could facilitate the transport of cationic species while favorably interacting with the fluorinated anions and reducing their mobility once incorporated onto the polymer networks.[15] We reasoned that the integration of ILs bearing fluorinated alkyl side chains onto the CGPEs could increase the Li ion conductivity by decreasing binding affinity of oxygen atoms on the glycol chains towards $Li^+$, while simultaneously improving $t_{Li}^+$ and electrochemical stability by immobilizing Li salt anion.[15] Accordingly, herein, we introduce a new type of gel polymer electrolyte (F-IL-GEL) composed of IL bearing a fluorinated alkyl side chain (F-IL), dipentaerythritol penta-/hexa-acrylate (DPEPA) and poly(ethylene glycol) methacrylate (PEGMA, average Mn = 500). From the design perspective, whereas PEGMA is used to achieve high ionic conductivity through the glycol chains, DPEPA enables the formation of a highly cross-linked gel network by means of abundant acrylate functional groups and pendant F-ILs were introduced to provide multiple features—namely, to effectively immobilize Li salt anion through noncovalent interactions with the Lewis acidic sites, to decrease the affinity of $Li^+$ towards oxygen atoms of glycol chains,[15] and to increase the electrochemical stability of the CGPE. In this direction, the integration of F-IL and the different crosslinking density of CGPEs were systematically investigated to demonstrate the unique role of F-IL to realize high $t_{Li}^+$, high Li ionic conductivity and enhanced electrochemical stability window.

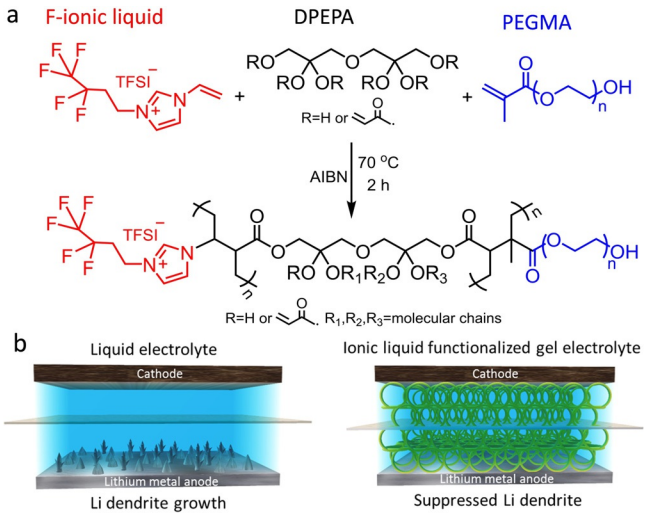


***Figure 1.*** Schematic representation of a) the synthesis of gel polymer electrolyte containing ionic liquid end groups and the proposed b) Li plating mechanism in liquid electrolyte (LE) and F-IL-GEL electrolyte.

## *Results and Discussion*

The F-IL was synthesized by reacting 1-vinylimidazole and 1,1,1,2,2-pentafluoro-4-iodobutane at 90 °C for 3 days. F-IL was isolated following an anion exchange with $TFSI^-$ (Figure S1a, S2).[16] In order to demonstrate the impact of fluorinated side chains, we also synthesized 3-butyl-1-vinyl-1*H*-imidazol-3-ium salt, IL, as a control sample by reacting 1-bromobutane and 1-vinylimidazole at 40 °C for 24 h and subsequently undergoing an anion exchange with the $TFSI^-$ anion (Figure S1b, S3).[17] The synthesis of the F-IL-GEL was completed by free radical polymerization of F-IL, DPEPA and PEGMA monomers in the liquid electrolyte (LE) of 1 M lithium bis(trifluoromethanesulfonyl)imide (LiTFSI) in 1,3-dioxolane (DOL) and 1,2-dimethoxyethane (DME) (1:1 by volume) with 2 wt % $LiNO_3$ additive. The as-prepared transparent solution was thermally initiated by using azobisisobutyronitrile (AIBN) at 70 °C through in situ radical polymerization of C=C bonds on the F-IL, DPEPA and PEGMA monomers to form F-IL-GEL.[18] As a comparison, we prepared two control samples—namely, IL-GEL, the fluorine-free counterpart incorporating 3-butyl-1-vinyl-1*H*-imidazol-3-ium, and GEL prepared by the polymerization of only DPEPA and PEGMA in the LE. Accordingly, we systematically investigated the effect of the IL end groups and the fluorinated alkyl chains in CGPEs in the context of promoting stable and uniform Li (de)plating.

Fourier-transform infrared spectra (FT-IR) measurements were conducted to verify the polymerization of F-IL, DPEPA and PEGMA monomers in F-IL-GEL. The peaks at $\approx 1633\ cm^{-1}$ in the DPEPA[19] and PEGMA,[20] and $\approx 3107\ cm^{-1}$ in the F-IL monomers were assigned to the stretching bands of C=C and C–H, respectively.[21] Upon polymerization, FT-IR spectrum of the F-IL-GEL showed (Figure 2a) a significant decrease in the intensity of the C=C stretching band pointing to the successful polymerization. The optimized ratio of the F-IL, DPEPA and PEGMA monomers, which was determined based on the formation of a gel, was found to be 2:4:1 by weight (Figure S4). In order to determine the critical gelation concentration, we used 1, 3 and 5 wt % of monomers in the LE for the polymerization reaction. Whereas 1 wt % monomers in the LE did not lead to the gel formation, we obtained homogenous translucent gels by using 3 and 5 wt % monomers (F-IL-GEL-3 % and F-IL-GEL-5 %) as verified by inverted (inset of Figure 2b) vial technique. We performed scanning electron microscopy (SEM) analysis to probe the morphology of the F-IL-GEL-3 % (Figures 2b and S5). The surface of the F-IL-GEL-3 % was found to be uneven and wrinkled, leading to the efficient uptake of the LE within the network. The mechanical strength of F-IL-GEL-3 % was measured by using a rheometer in a plate-plate (0.5 mm gap) setting. The sample was prepared by putting the monomer solution on the bottom-plate and in situ polymerizing between two plates at 70 °C for 2 hours. The shear modulus of F-IL-GEL-3 % was found to be 2500 Pa (Figure S6). Since thermal stability and volatility of an electrolyte are crucial for the battery safety, we compared the thermal stability of the F-IL-GEL-3 % and LE using thermogravimetric analysis (TGA) in the temperature range from 25 °C to

  

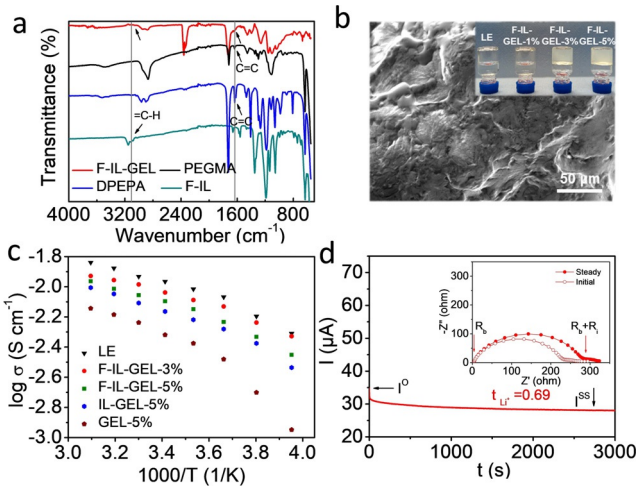


***Figure 2.*** a) FT-IR spectra of F-IL, DPEPA and PEGMA monomers and the F-IL-GEL. b) SEM image of the F-IL-GEL-3%. (Inset) The optical images of LE, F-IL-GEL-1%, F-IL-GEL-3% and F-IL-GEL-5%. c) Temperature dependent ionic conductivity plots of LE, F-IL-GEL-3%, F-IL-GEL-5%, IL-GEL-5% and GEL-5%. d) The chronoamperometry profile of Li|F-IL-GEL-3%|Li cell under a polarization voltage of 10 mV. (Inset) The corresponding electrochemical impedance spectra (EIS) before and after polarization.

300 °C at a heating rate of 5 °C min$^{-1}$ (Figure S7). As expected, while the LE rapidly evaporated, F-IL-GEL-3% showed a very small mass loss (4.5 wt%) below 100 °C, thus verifying its superior thermal stability and efficient uptake of the LE within the cross-linked polymer network.

The simultaneous realization of high ionic conductivity and $t_{Li}^{+}$ in CGPEs is highly desirable for their practical use in LMBs, but is rather challenging to achieve in practice. Accordingly, we compared (Figure 2c) the ionic conductivities of the prepared electrolytes at different temperatures. The ionic conductivities of GEL-5% and IL-GEL-5% were $4.80\times10^{-3}$ and $6.86\times10^{-3}$ S cm$^{-1}$ at 20 °C, respectively, which were lower than those of F-IL-GEL-5% ($8.01\times10^{-3}$ S cm$^{-1}$) and F-IL-GEL-3% ($9.16\times10^{-3}$ S cm$^{-1}$) at the same temperature. Notably, the ionic conductivity of F-IL-GEL-3% is the highest among all the CGPEs and is even close to that of the LE ($1.08\times10^{-2}$ S cm$^{-1}$). Such high ionic conductivity of F-IL-GEL-3% could be attributed to the introduction of ionic liquid segments incorporating fluorinated side chains as verified by the gradual increase in the ionic conductivity going from GEL-5% to IL-GEL-5% to F-IL-GEL-3%. Based on the rationale that the higher $t_{Li}^{+}$ value leads to a longer time for Li dendrite initiation according to the Sand's time formula,[22] we also calculated the $t_{Li}^{+}$ of different CGPEs to demonstrate the effect of F-IL. The $t_{Li}^{+}$ value of the F-IL-GEL-3% and F-IL-GEL-5% reached 0.69 and 0.41 (Figures 2d and S8a), respectively, which is significantly higher than those of the IL-GEL-5% (0.35), GEL-5% (0.26) and LE (0.25) (Figures S8b–d). The marked improvement of $t_{Li}^{+}$ for F-IL-GEL arises from the inherent Lewis acidity of the polymer backbone to immobilize the TFSI anion, which promotes the Li cation mobility. Higher F-IL content, however, does not seem to be beneficial considering the lower $t_{Li}^{+}$ of F-IL-GEL-5% compared to that of F-IL-GEL-3%, which suggests that there is an optimum F-IL content and that higher F-IL content could interfere with the $Li^{+}$ transport through Coulombic repulsion. These results point to the fact that the incorporation of F-IL to the CGPE boosts both the ionic conductivity and $t_{Li}^{+}$ simultaneously, a challenging task in developing electrolytes, which is also proven by the deshielding of $^{7}$Li peak in the $^{7}$Li solid-state NMR spectrum of F-IL based polymer electrolyte compared to that of IL based one (Figure S9).

Morphology evolutions and structural stability of Li plating on the Cu foil with the LE, F-IL-GEL-3% and F-IL-GEL-5% were investigated (Figures 3a–c). The SEM image of Li|LE|Cu cell, with 5 mAh cm$^{-2}$ Li plating at 0.5 mA cm$^{-2}$, showed a nonuniform morphology with massive holes. Moreover, the cross-sectional SEM analysis revealed the thickness of the Li plating layer is ≈46 μm with a loose structure (Figure 3a, inset). In comparison, the surface of the Li plating turned out to be smooth in the cell with F-IL-GEL-3% when tested under the same conditions, and the thickness decreased to ≈28 μm, which is close to the theoretically expected value of 25 μm for the case of pure metallic Li upon the same amount of Li plating (Figure 3b, inset). When we tested F-IL-GEL-5%, the morphology of the Li metal exhibited a thicker Li deposition layer of ≈35 μm (Figure 3c, inset). The high magnification SEM images of the plated Li with the LE, F-IL-GEL-3% and F-IL-GEL-5% CGPEs are presented in Figure S10a–c. In order to further evaluate the structural stability of Li metal anode, we conducted a plating/stripping for 50 cycles with a capacity of 2 mAh cm$^{-2}$ at 1 mA cm$^{-2}$ under a Li|Li symmetric cell configuration. We observed the formation of cracks on the surface of the Li metal in the cell with the LE and F-IL-GEL-5%, resulting from a nonhomogeneous Li deposition (Figures 3d,f, S11a and S11c). On the contrary, the cell with F-IL-GEL-3% exhibited a relatively uniform, smooth and dense morphology of Li deposit (Figures 3e and S11b). The changes in the Li metal anode surface morphology agreed nicely with the trend

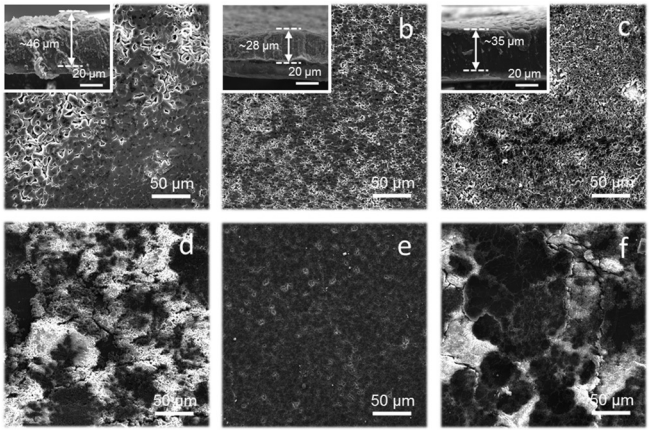


***Figure 3.*** a–c) Top and cross-sectional SEM images of plated Li with a capacity of 5 mAh cm$^{-2}$ Li on Cu substrate at 0.5 mA cm$^{-2}$ with a) LE, b) F-IL-GEL-3% and c) F-IL-GEL-5%. d–f) The morphology of Li anodes after 50 cycles at 1 mA cm$^{-2}$ with a cut-off capacity of 2 mAh cm$^{-2}$ in d) Li|LE|Li, e) Li|F-IL-GEL-3%|Li, and f) Li|F-IL-GEL-5%|Li cells.

  

in $t_{Li}^{+}$. The F-IL-GEL-3% effectively reduced anion mobility, giving rise to high $Li^{+}$ mobility and conductivity, thus effectively suppressing Li dendrite growth.

Linear sweep voltammetry (LSV) analysis was conducted at a scan rate of 0.1 mV s$^{-1}$ to probe the electrochemical stability window of the LE and the prepared CGPEs (Figure S12 and S13). The LE (DOL/DME) started to become unstable at 4.00 V and showed a serious decomposition at about 4.20 V.[23] The instability of LE largely originates from the relatively unstable cyclic structure of DOL.[24] In the case of GEL, the onset potential for the decomposition was found to be higher than 4.00 V pointing to the encapsulation of electrolyte within the GEL structure. Notably, the introduction of ILs led to a significant improvement in the electrochemical stability window up to 4.55 V for both IL-GEL-3% and F-IL-GEL-3%. This enhancement is attributed to the electrostatic and hydrogen bonding interactions between IL and $TFSI^{-}$ anion, which in turn retards the decomposition of anion.[25] These findings were further verified by the cyclic voltammetry (CV) analyses of F-IL-GEL-3% and LE, which were found to be in a good agreement with the LSV analysis results (Figure S14). In the potential range between −1.0 V and 1.0 V versus $Li^{+}$/Li, reduction and oxidation peaks were observed, which stemmed from the reversible plating and stripping of metallic Li.[26] The stability window up to 4.55 V for the F-IL-GEL would play an important role in employing high voltage cathode materials in practical LMBs.

Electrochemical cycling stability of symmetric Li | Li cells was investigated at different current densities. Under a current density of 2 mA cm$^{-2}$ with an areal capacity of 2 mAh cm$^{-2}$, the voltage hysteresis increased sharply at only around 50 h for the cell with LE, indicating unstable interface caused by the uncontrolled Li-dendrite growth. On the contrary, the symmetrical cell based on F-IL-GEL-3% maintained a flat voltage plateau and reduced overpotential of 26 mV for 400 cycles (860 h). Due to the decreased ionic conductivity, the symmetric cell with F-IL-GEL-5% delivered a steady but higher voltage hysteresis of 46 mV (Figure S15).

We also tested cycling performance for symmetric cells with an areal capacity of 9 mAh cm$^{-2}$ under the current density of 3 mA cm$^{-2}$ to evaluate the practical viability of CGPEs (Figure 4a). Smooth Li stripping/plating plateaus were achieved with the F-IL-GEL-3% protected lithium anode even after 1800 h during 300 cycles. The voltage hysteresis without obvious oscillation kept the overpotential within 24 mV, which was smaller than the cell with F-IL-GEL-5% of 52 mV. In contrast, the failure of the cell occurred in only 100 h with a sharp overpotential increase for LE, due to the rapid growth of dendrites and thicker SEI layer formation. Li | Li symmetrical cells with each electrolyte were further evaluated at different current rates (Figure S16). The symmetrical cell using F-IL-GEL-3% exhibited the smallest and stable polarization at 5 mA cm$^{-2}$ of 5 mAh cm$^{-2}$ capacity, verifying its ability toward suppressing Li dendrites at high current densities. Furthermore, electrochemical impedance spectroscopy (EIS) analyses were conducted for Li | LE | Li, Li | F-IL-GEL-3% | Li and Li | F-IL-GEL-5% | Li symmetric cells after cycling at 3 mA cm$^{-2}$ with a cut-off capacity of 9 mAh cm$^{-2}$ at different cycling times to evaluate the interfacial stability (Figure S17). During the initial 36 h, F-IL-GEL-5% showed the largest interfacial resistance ($R_f$) of 10.3 Ω originating from the lowest ionic conductivity and dense polymer backbone. When the cycling time was increased to 150 h, the $R_f$ of Li | LE | Li significantly increased to 19.94 Ω due to the accumulated thick SEI associated with uncontrolled Li dendrite growth.[27] In stark contrast to LE and F-IL-GEL-5%, F-IL-GEL-3% maintained a low and stable $R_f$ of 2.16 Ω without obvious oscillation (Table S1). These results indicate that there is an optimum crosslinking density to achieve stable interface and low polarization on LMA. Electrode | electrolyte interphases were characterized by X-ray photoelectron spectroscopy (XPS) analysis after 20 cycles (Figure S18 and S19). In the C1s spectra, the higher intensity of C–O and C–C components in the gel-based electrolytes compared to the LE originates from the remaining polymer on the Li metal surface. After 1 min of sputtering, most of the remaining polymer was etched. In the F1s spectra, we observed both TFSI anion and LiF on the Li surface. The F-IL-GEL-3% showed the highest $CF_3$ signal, owing to the trapping of TFSI anion in the polymer network. Moreover, the highest LiF content in the case of F-IL-GEL-3% observed after sputtering explains the stable interphase information and uniform Li plating. FT-IR and SEM analyses were conducted to evaluate the stability of F-IL-GEL-3% during cycling (Figure S20 and S21). The results indicated highly consistent chemical identity of F-IL-GEL-3% after cycling, implying its (electro)chemical stability.

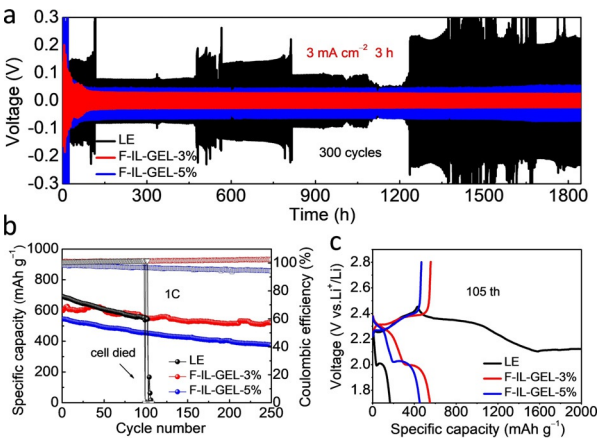


***Figure 4.*** a) Voltage-time profiles of symmetric cells with LE, F-IL-GEL-3% and F-IL-GEL-5% when measured at 3 mA cm$^{-2}$ with 9 mAh cm$^{-2}$. b) Cycling performance and CEs of Li-S cells with LE, F-IL-GEL-3% and F-IL-GEL-5% at 1 C. c) Galvanostatic discharge-charge profiles at 105th cycle for the three Li-S cells.

Considering the ability of ILs to immobilize anions, the CGPEs were applied for lithium-sulfur (Li-S) batteries in order to mitigate the polysulfide shuttling, which is a major cause of capacity decay. Towards this end, the $Li_2S_8$ permeation test was performed to compare the polysulfide migration in different electrolytes (Figure S22). After 4 h, F-IL-GEL-3% showed a minor polysulfide diffusion, thus showing its ability to block polysulfide migration. On the contrary, LE showed complete diffusion of polysulfides. In order to evaluate the electrochemical performance of CGPEs in Li-S

  

batteries, we employed pre-plated Li on Cu foil as an anode with an areal capacity of 3 mAh cm$^{-2}$, and coupled it with a sulfur cathode with ketjen black. Li-S cells using LE, F-IL-GEL-3 % and F-IL-GEL-5 % were cycled at a constant rate of 1 C (1675 mA g$^{-1}$ or 1.67 mA cm$^{-2}$) to evaluate the influence of the gel polymer electrolytes (Figure 4b). After 250 cycles, the cell with F-IL-GEL-3 % exhibited a reversible capacity of 519.3 mAh g$^{-1}$, while the discharge capacity of the cell with F-IL-GEL-5 % was only 373.1 mAh g$^{-1}$ with a constant falling of CE, ascribed to the increased kinetic barrier caused by the lower $t_{Li}^{+}$ and ionic conductivity. In contrast, the cell based on LE cycled only for 105 cycles, which exhibited failed charging curves without achieving the cut-off voltage (Figure 4c). This phenomenon was caused by the Li dendrite growth and consequent short-circuits, which is consistent with the sudden voltage fluctuations in the above symmetric Li | Li cell tests. During the initial 100 cycles, the cells based on the F-IL-GEL-3 % and F-IL-GEL-5 % showed higher capacity retention (92.4 % and 83.4 %) compared to that of the LE (79.5 %), indicating homogenous Li plating and suppression of polysulfide shuttling during Li-S full cell cycling by the introduction of the fluorinated ionic liquids to the gel electrolyte. While the cells employing gel electrolytes showed superior capacity retention, their capacity was found to be lower than that of LE. In order to understand the capacity difference between LE and CGPEs, we compared the discharge profiles at 1$^{st}$ and 31$^{st}$ cycles (Figure S23).[28] The first plateau at 2.3 V, which corresponds to the formation of polysulfides, $Li_2S_8$, and sulfur utilization, was clearly observed for all the electrolytes and found to be extended for F-IL-GEL-3 %. The second plateau originating from the conversion of soluble $Li_2S_8$ to $Li_2S_4$ and $Li_2S_2$, however, was shortened for both F-IL-GEL-3 % and -5 %, which was attributed to the slower mass transport of sulfur redox intermediates, thus explaining the lower capacity of CGPEs compared to the LE. This effect was more pronounced in the case of F-IL-GEL-5 % as evidenced by the lower capacity compared to the F-IL-GEL-3 % presumably due to its higher crosslinking density. Li-S full cell with F-IL-GEL-3 % exhibited superior performance at high rates which largely maintained its capacity during cycling at different C-rates, while Li-S cell with LE lost its capacity during the same cycling process (Figure S24).

## Conclusion

We demonstrated a new type of cross-linked gel polymer electrolyte containing imidazolium ionic liquid end groups bearing a fluorinated alkyl chain, providing both high ionic conductivity and high Li ion transference number. Specifically, these exceptional properties were enabled by the Lewis acidic nature of the polymer backbone that reduced the mobility of Li salt anion, and played a crucial role for uniform Li plating and for restraining Li dendrite growth during cycling. This study highlights the impact of molecular level engineering of polymer gel electrolytes in controlling the two critical parameters, $Li^+$ conductivity and transference number, to achieve stable cycling of Li metal anodes and can be expanded to other metallic anode systems that suffer similarly from dendrite growth and interfacial instability.

## Acknowledgements

A.C. acknowledges the support from the Swiss National Science Foundation (SNF) for funding of this research (200021-188572). J.W.C. acknowledges the support by the National Research Foundation of Korea (NRF) grants (NRF-2021R1A2B5B03001956 and NRF-2018M1A2A2063340), the Technology Innovation Program (20012341) funded by the Ministry of Trade, Industry & Energy (MOTIE) of Korea and generous support from the Institute of Engineering Research (IOER) and Inter-university Semiconductor Research Center (ISRC) at Seoul National University. We would like to thank Dr Mario El Kazzi at PSI for XPS analysis and Dr Véronique Trappe at University of Fribourg for rheology analysis.

## Conflict of Interest

The authors declare no conflict of interest.

**Keywords:** gel polymer electrolyte · ionic conductivity · ionic liquid · Li ion transference number · Li metal anode

[1] a) J. M. Tarascon, M. Armand, *Nature* **2001**, *414*, 359 – 367; b) X. B. Cheng, R. Zhang, C. Z. Zhao, Q. Zhang, *Chem. Rev.* **2017**, *117*, 10403 – 10473; c) J. W. Choi, D. Aurbach, *Nat. Rev. Mater.* **2016**, *1*, 16013; d) P. G. Bruce, S. A. Freunberger, L. J. Hardwick, J.-M. Tarascon, *Nat. Mater.* **2012**, *11*, 19 – 29.

[2] a) M. D. Tikekar, S. Choudhury, Z. Tu, L. A. Archer, *Nat. Energy* **2016**, *1*, 16114; b) D. Lin, Y. Liu, Y. Cui, *Nat. Nanotechnol.* **2017**, *12*, 194 – 206; c) D. Lin, Y. Liu, A. Pei, Y. Cui, *Nano Res.* **2017**, *10*, 4003 – 4026.

[3] a) J. Zheng, M. H. Engelhard, D. Mei, S. Jiao, B. J. Polzin, J.-G. Zhang, W. Xu, *Nat. Energy* **2017**, *2*, 17012; b) H. Dai, K. Xi, X. Liu, C. Lai, S. Zhang, *J. Am. Chem. Soc.* **2018**, *140*, 17515 – 17521; c) T. Zhou, Y. Zhao, M. El Kazzi, J. W. Choi, A. Coskun, *ACS Energy Lett.* **2021**, *6*, 1711 – 1718.

[4] a) G. Wang, C. Chen, Y. Chen, X. Kang, C. Yang, F. Wang, Y. Liu, X. Xiong, *Angew. Chem. Int. Ed.* **2020**, *59*, 2055 – 2060; *Angew. Chem.* **2020**, *132*, 2071 – 2076; b) T. Zhou, Y. Zhao, J. W. Choi, A. Coskun, *Angew. Chem. Int. Ed.* **2019**, *58*, 16795 – 16799; *Angew. Chem.* **2019**, *131*, 16951 – 16955; c) C. Yan, X. B. Cheng, Y. Tian, X. Chen, X. Q. Zhang, W. J. Li, J. Q. Huang, Q. Zhang, *Adv. Mater.* **2018**, *30*, 1707629; d) Y. Liu, D. Lin, P. Y. Yuen, K. Liu, J. Xie, R. H. Dauskardt, Y. Cui, *Adv. Mater.* **2017**, *29*, 1605531.

[5] a) C.-P. Yang, Y.-X. Yin, S.-F. Zhang, N.-W. Li, Y.-G. Guo, *Nat. Commun.* **2015**, *6*, 8058; b) D. Lin, Y. Liu, Z. Liang, H.-W. Lee, J. Sun, H. Wang, K. Yan, J. Xie, Y. Cui, *Nat. Nanotechnol.* **2016**, *11*, 626 – 632; c) Q. Yun, Y.-B. He, W. Lv, Y. Zhao, B. Li, F. Kang, Q.-H. Yang, *Adv. Mater.* **2016**, *28*, 6932 – 6939.

[6] F. Han, J. Yue, C. Chen, N. Zhao, X. Fan, Z. Ma, T. Gao, F. Wang, X. Guo, C. Wang, *Joule* **2018**, *2*, 497 – 508.

[7] D. Lei, Y.-B. He, H. Huang, Y. Yuan, G. Zhong, Q. Zhao, X. Hao, D. Zhang, C. Lai, S. Zhang, *Nat. Commun.* **2019**, *10*, 4244.

[8] X. Cheng, J. Pan, Y. Zhao, M. Liao, H. Peng, *Adv. Energy Mater.* **2018**, *8*, 1702184.

[9] D. Zhou, D. Shanmukaraj, A. Tkacheva, M. Armand, G. Wang, *Chem* **2019**, *5*, 2326 – 2352.

  

[10] G. Li, Y. Gao, X. He, Q. Huang, S. Chen, S. H. Kim, D. Wang, *Nat. Commun.* **2017**, *8*, 850.
[11] a) L. Porcarelli, A. S. Shaplov, F. Bella, J. R. Nair, D. Mecerreyes, C. Gerbaldi, *ACS Energy Lett.* **2016**, *1*, 678 – 682; b) D. M. Shin, J. E. Bachman, M. K. Taylor, J. Kamcev, J. G. Park, M. E. Ziebel, E. Velasquez, N. N. Jarenwattananon, G. K. Sethi, Y. Cui, *Adv. Mater.* **2020**, *32*, 1905771.
[12] a) C. Wang, A. Wang, L. Ren, X. Guan, D. Wang, A. Dong, C. Zhang, G. Li, J. Luo, *Adv. Funct. Mater.* **2019**, *29*, 1905940; b) P. Jaumaux, Q. Liu, D. Zhou, X. Xu, T. Wang, Y. Wang, F. Kang, B. Li, G. Wang, *Angew. Chem. Int. Ed.* **2020**, *59*, 9134 – 9142; *Angew. Chem.* **2020**, *132*, 9219 – 9227.
[13] Y. Lu, K. Korf, Y. Kambe, Z. Tu, L. A. Archer, *Angew. Chem. Int. Ed.* **2014**, *53*, 488 – 492; *Angew. Chem.* **2014**, *126*, 498 – 502.
[14] D. O'Hagan, *Chem. Soc. Rev.* **2008**, *37*, 308 – 319.
[15] D. H. Wong, J. L. Thelen, Y. Fu, D. Devaux, A. A. Pandya, V. S. Battaglia, N. P. Balsara, J. M. DeSimone, *Proc. Natl. Acad. Sci. USA* **2014**, *111*, 3327 – 3331.
[16] D. Rauber, F. Heib, M. Schmitt, R. Hempelmann, *J. Mol. Liq.* **2016**, *216*, 246 – 258.
[17] C. Yuan, J. Guo, F. Yan, *Polymer* **2014**, *55*, 3431 – 3435.
[18] M. Liu, D. Zhou, Y.-B. He, Y. Fu, X. Qin, C. Miao, H. Du, B. Li, Q.-H. Yang, Z. Lin, T. S. Zhao, F. Kang, *Nano Energy* **2016**, *22*, 278 – 289.
[19] H. Zhang, J. Ou, Y. Wei, H. Wang, Z. Liu, L. Chen, H. Zou, *Anal. Chim. Acta* **2015**, *883*, 90 – 98.
[20] M. Zaheer, H. Xu, B. Wang, L. Li, Y. Deng, *J. Electrochem. Soc.* **2020**, *167*, 070504.
[21] M. V. Reddy, K. R. Byeon, S. H. Park, D. W. Kim, *Tetrahedron* **2017**, *73*, 5289 – 5296.
[22] H. J. Sand, *Phil. Mag.* **1901**, *1*, 45 – 79.
[23] F.-Q. Liu, W.-P. Wang, Y.-X. Yin, S.-F. Zhang, J.-L. Shi, L. Wang, X.-D. Zhang, Y. Zheng, J.-J. Zhou, L. Li, *Sci. Adv.* **2018**, *4*, eaat5383.
[24] H. Zhong, C. Wang, Z. Xu, F. Ding, X. Liu, *Sci. Rep.* **2016**, *6*, 1 – 7.
[25] a) Y. Wang, L. Fu, L. Shi, Z. Wang, J. Zhu, Y. Zhao, S. Yuan, *ACS Appl. Mater. Interfaces* **2019**, *11*, 5168 – 5175; b) C. H. Park, D. W. Kim, J. Prakash, Y.-K. Sun, *Solid State Ionics* **2003**, *159*, 111 – 119; c) C. F. Marchiori, R. P. Carvalho, M. Ebadi, D. Brandell, C. M. Araujo, *Chem. Mater.* **2020**, *32*, 7237 – 7246; d) W. Zhou, S. Wang, Y. Li, S. Xin, A. Manthiram, J. B. Goodenough, *J. Am. Chem. Soc.* **2016**, *138*, 9385 – 9388.
[26] Q. Lu, Y. B. He, Q. Yu, B. Li, Y. V. Kaneti, Y. Yao, F. Kang, Q. H. Yang, *Adv. Mater.* **2017**, *29*, 1604460.
[27] H. Chen, A. Pei, D. Lin, J. Xie, A. Yang, J. Xu, K. Lin, J. Wang, H. Wang, F. Shi, *Adv. Energy Mater.* **2019**, *9*, 1900858.
[28] G. L. Shebert, S. Zamani, C. Yi, Y. L. Joo, *J. Mater. Chem. A* **2020**, *8*, 4341 – 4353.

Manuscript received: May 8, 2021
Accepted manuscript online: August 11, 2021
Version of record online: September 7, 2021

  